Optics and Lasers in Engineering 51 (2013) 514–519

Contents lists available at SciVerse ScienceDirect

Optics and Lasers in Engineering

journal homepage: www.elsevier.com/locate/optlaseng

Accurate calibration for 3D shape measurement system using a binary defocusing technique

Leah Merner, Yajun Wang, Song Zhang*

Mechanical Engineering Department, Iowa State University, Ames, IA 50011, United States

ARTICLE INFO

Article history:
Received 6 July 2012
Received in revised form
16 September 2012
Accepted 28 October 2012
Available online 24 November 2012

Keywords:
Calibration
Structured light
3D shape measurement
Phase shifting
Defocusing

ABSTRACT

This paper introduces a novel method to calibrate 3D shape measurement systems that use the binary defocusing technique. Specifically, this method calibrates the pixelwise z as low-order polynomial functions of absolute phase; (x, y) coordinates are calculated from camera calibration with known z value; and the camera is calibrated using the standard flat checkerboard method. Because this method does not require estimation of the projector's parameters, it can be adopted for any phase measurement system including those employing out-of-focus projectors. Our experiment found that the root-mean-squared (rms) error for the depth measurement is less than 70 μm when the measurement depth range is about 100 mm, which is at the same level of the calibration stage ± 50 μm.

1. Introduction

Precise measurement applications in manufacturing and medical sciences increasingly integrate real-time 3D shape measurement systems based on digital sinusoidal fringe projection. A digital fringe projection (DFP) technique projects a sequence of sinusoidal structured patterns onto an object and captures the deformed pattern images. The 2D images can then be used to generate a 2D phase map from which the 3D information for each pixel can be uniquely extracted. The DFP technique offers good measurement accuracy, improves computation speed over many other 3D shape measurement techniques, and eliminates image matching difficulties of traditional stereo-vision systems by replacing one camera with a projector [1]. These advances in 3D shape measurement create opportunities for application of digital fringe technologies in high precision measurement. However, the drawbacks of a conventional DFP technique include projector nonlinear gamma errors, difficult synchronization between projector and camera, and speed limitations of the projector, which may drastically affect measurement quality [2].

To avoid the problems caused by the conventional DFP technique projection technique, Lei and Zhang recently proposed a structured light technique that projects defocused binary structured patterns instead of sinusoidal patterns [3]. The binary defocusing technique could alleviate the problems of conventional DFP techniques in that the projector nonlinearity does not affect measurement accuracy, the time modulation effect of the digital light-processing (DLP) technique is less sensitive to precise synchronization, and 1-bit instead of 8-bit data transfer reduces DLP projector's processing power demand [4].

However, the binary defocusing technique introduces a new challenge: calibrating such a system becomes more difficult because of the use of an out-of-focused projector since most well-established, accurate calibration methods for structured light systems require the projector to be in focus (e.g. the least squares [5,6], projector image regeneration [7–10], and camera-projector system optimization [11–13]). The calibration accuracy usually determines the accuracy of a 3D shape measurement system; thus, an accurate calibration method is vital to any precision 3D shape measurement system. The reference-plane based phase-to-height conversion methods [14] could be used if the depth measuring range is small [7]. However, the calibration accuracy is low if the measuring depth range is large. Therefore, a new calibration technique must be developed for the binary defocusing technique before it can be extensively adopted.

We propose a novel method for accurately calibrating a 3D shape measurement system using the binary defocusing technique by a method that indirectly calibrates the defocused projector. Specifically, the proposed method includes two stages: depth z calibration and (x, y) coordinates calibration. The first stage is calibrating z coordinate information by translating a calibration plane over known depths, recording the depth z values and absolute phase values per pixel for each plane, and fitting a curve for each pixel across the entire depth range to establish the depth

* Corresponding author. Tel.: +1 515 294 0723; fax: +1 515 294 3261.
E-mail addresses: song@iastate.edu, isusong@gmail.com (S. Zhang).

0143-8166/$ - see front matter © 2012 Elsevier Ltd. All rights reserved.
http://dx.doi.org/10.1016/j.optlaseng.2012.10.015

z and the absolute phase. We found that the depth z per pixel can be described as 3rd- or 4th-order polynomials of the absolute phase value; therefore, the depth z can be accurately recovered once the polynomial functions are calibrated. The second stage is to calibrate (x, y) coordinates, which is a standard camera calibration method. We employed the checkerboard camera calibration method proposed by Zhang [15] and estimated the camera's intrinsic and extrinsic parameters using the Matlab software package developed by Bouguet [16]. If the camera calibration depth z is aligned with the first calibration procedure, (x, y) coordinates can be computed using the calibrated camera parameters. Our experiment found that the root-mean-squared (rms) error for the depth measurement is less than 70 μm, which is at the same level of the calibration stage ± 50 μm.

After submitting this paper, we found a technique proposed by Sitnik et al. [26] that presented a very similar idea to ours. In that paper, it did point-by-point polynomial fitting for depth z calibration, and utilized the least square method for (x, y) calibration. It concluded that 5th or higher-order polynomials are required for depth z calibration. However, the method proposed by Sitnik was used to handle conventional sinusoidal fringe projection method, which is different from the main focus this paper: calibrating a system using the binary defocusing technique. Our experimental finding is slightly different from Sitnik's paper in that only 3rd- or 4th-order polynomials are necessary. This might result from different fringe pattern generation techniques. In addition, we adopted the checkerboard calibration method for (x, y) calibration. This calibration method is well developed and can also easily consider lens distortion influence, thus has the potential to provide more accurate calibration results compared with the least-square method adopted in Ref. [26].

Section 2 explains the principles used for the proposed calibration technique. Section 3 describes the experimental setup and method. Section 4 shows the experimental results. Finally, Section 5 summarizes this paper.

2. Principle

2.1. Nine-step phase-shifting algorithm

Phase-shifting algorithms are widely used in optical metrology because of their measurement speed and accuracy [17]. Numerous phase-shifting algorithms have been developed including three-step, four-step, double-three-step, and five-step algorithms. In this research, we use a nine-step phase-shifting algorithm to reduce the influence of random noises and high-frequency harmonics during defocusing. The nine phase-shifted fringe images can be described as

$$I_n(x,y) = I'(x,y) + I''(x,y)\cos(\phi + 2\pi n/9), \tag{1}$$

where $I'(x,y)$ is the average intensity, $I''(x,y)$ the intensity modulation, $\phi(x,y)$ the phase to be solved for, and $n=1,2,\ldots,9$. The phase, $\phi(x,y)$ can be solved for as follows:

$$\phi(x,y) = \tan^{-1}\left[\frac{\sum_{n=1}^{9} I_n(x,y)\sin(2\pi n/9)}{\sum_{n=1}^{9} I_n(x,y)\cos(2\pi n/9)}\right]. \tag{2}$$

Eq. (2) provides the phase ranging $[-\pi, \pi)$ with 2π discontinuities. This 2π phase jumps can be removed to obtain the continuous phase map by adopting a phase unwrapping algorithm, such as one of the algorithms described in Book [18]. The phase unwrapping is essentially to determine the locations of the phase jumps and remove them by adding or subtracting multiples of 2π. However, the phase obtained by a spatial phase unwrapping is relative phase. In this research, absolute phase is required for accurate calibration.

2.2. Absolute phase recovery with gray coding

The conventional unwrapping method only recovers the relative phase for each pixel. It is sensitive to noise and cannot measure step heights greater than π, which may introduce large measurement errors. Instead, recovering the absolute phase, $\Phi(x,y)$, can avoid these errors and provide a more robust solution. Methods such as two- or multi-wavelength [19,20], optimal multifrequency [21], temporal phase-unwrapping [22], and gray-coding plus phase-shifting [23] methods can recover the absolute phase. This paper uses the gray-coding plus phase-shifting method to obtain the fringe order for absolute phase retrieval in order to maintain the merits of the binary defocusing technique where only binary patterns are needed. Specifically, a sequence of designed binary coding patterns uniquely defines the location of each 2π phase jump to create a fringe order, $k(x, y)$, so that the phase can be recovered pixel by pixel by referring to the binary coded patterns.

$$\Phi(x,y) = \phi(x,y) + k(x,y) \times 2\pi. \tag{3}$$

2.3. Establishment of the relationship between absolute phase and depth

Previous research has shown that the absolute phase and the depth are monotonically related per camera pixel [4]. Therefore, geometrical models can describe the relationship between the absolute phase and the depth, and vice versa [24]. Then the calibration process is to retrieve the parameters in the models. However, due the complexity of the real projection system, the models are always not very accurate with some assumptions, which would bring errors for the final calibration accuracy. Previous research found that this relationship of the absolute phase and the depth is non-linear and can be approximated with low-order polynomials [4,26]

$$z(x,y) = \sum c_k(x,y) \cdot \Phi(x,y)^k. \tag{4}$$

Here $c_k(x,y)$ are constants to be estimated by calibration.

Fig. 1 shows absolute phase and depth are related monotonically and nonlinearly, verifying that curve fitting calibration could accurately describe depth z coordinate information.

In our experiments, five different curve fitting cases were examined: linear interpolation, 2nd-, 3rd-, and 4th-order polynomials. The remaining experiments for this paper use the best performing fitting method. It is interesting to note that Zhang et al. proposed a calibration technique that uses linear interpolation to define the relationship between *relative phase* and depth

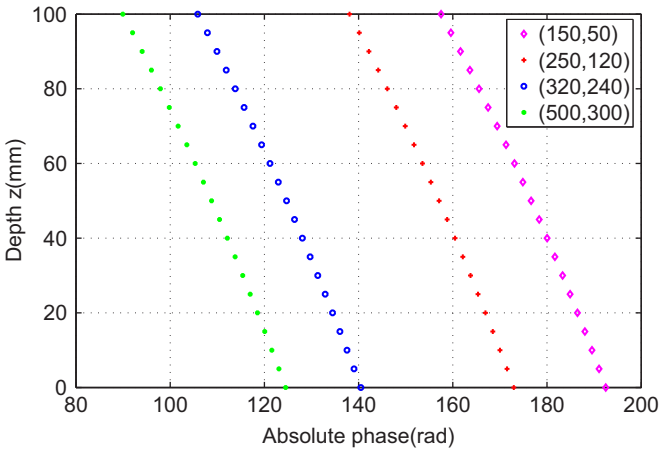

Fig. 1. Absolute phase $\Phi(x,y)$ vs. depth z for four arbitrary pixels.

[25]. This technique could provide good accuracy if the increments between calibration planes are small enough (i.e., the nonlinear curves can be approximated as linear segments). However, as shown in Fig. 1, the relationship between phase and depth is nonlinear and other curve fitting methods could generate better calibration accuracy. By fitting a curve across all calibration planes that define the depth range, the z coordinate can be accurately calibrated per pixel.

2.4. Camera parameters estimation for x and y calibration

Typically, the pinhole camera model describes a camera with intrinsic parameters, such as focal length, principle point, pixel skew factor; and extrinsic parameters defining camera rotation and translation between a world coordinate system used to unify x, y and z calibration and the camera coordinate system [15]. A 3D point in world coordinate system can be denoted by $M=[x,y,z]^T$, and the corresponding 2D point in camera coordinate system is $m=[\mu,v]^T$. By adding 1 as the last element, the augmented vectors are: $\tilde{M}=[x,y,z,1]^T$ and $\tilde{m}=[\mu,v,1]^T$. The relationship between a 3D point $\tilde{M}$ and its image projection m is given by

$$s\tilde{m}=A[R\ \ T]\tilde{M}, \tag{5}$$

where s is a scale factor, $[R, T]$ is the extrinsic matrix, R is the 3×3 rotation matrix, and T is the translation vector. A is the camera intrinsic matrix that can be described as

$$A=\begin{bmatrix}\alpha & \gamma & \mu_0\\ 0 & \beta & v_0\\ 0 & 0 & 1\end{bmatrix}. \tag{6}$$

Here α and β are respectively the focal lengths along x and y axis, γ is the camera skew factor, and (u_0,v_0) is the principal point where the optical axis intersects with the camera sensor.

Once the extrinsic and intrinsic matrices are determined through calibration, the world coordinate system and camera coordinate system can be accurately matched. If camera parameters are obtained, x and y information can be determined by

$$s\begin{bmatrix}\mu\\ v\\ 1\end{bmatrix}=A[R,\ T]\begin{bmatrix}x\\ y\\ z\\ 1\end{bmatrix}. \tag{7}$$

In this equation, because z is a known value obtained through a curve fitting procedure, (x, y) can be uniquely solved. Because this technique does not require precise determination of the corresponding projector pixel, it can be used to calibrate any phase measurement system including the DFP system with projector being out-of-focus. It should be noted that direct projector calibration is not required; thus, the technique can be applied to any phase measurement system.

3. Experiments

3.1. System setup

The structured light system used in our experiments consisted of a digital-light-processing (DLP) projector (Samsung SP-P310MEMX) and digital USB charge-coupled-device (CCD) camera (Jai Pulnix TM-6740CL). The camera uses a 16 mm focal length Mega-pixel lens (Computar M1614-MP). The camera resolution is 640×480 with a maximum frame rate of 200 frames/s. The projector has a resolution of 800×600 with a projection distance of 0.49–2.80 m. Fig. 2 shows the calibration system setup. The field of view of the projector and camera are respectively 405 mm $\times$ 295 mm and 220 mm $\times$ 160 mm.

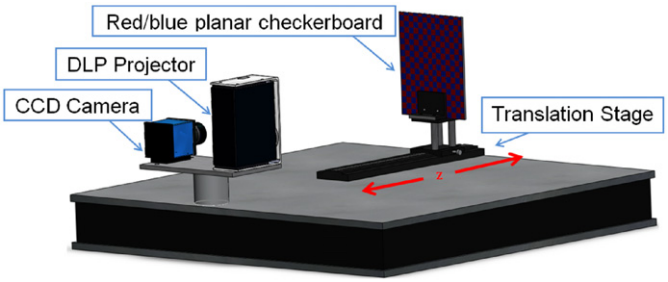

Fig. 2. Calibration system setup.

The projector projected fringe pattern onto a laser-printed red/blue checkerboard pattern attached to a nearly planar surface. The planar surface was attached to a precision TECHSPEC Metric long travel linear translation stage. The stage is 250 mm long with a traveling accuracy of ± 0.05 mm. The flat object with red/blue checkerboard attached is mounted on top of the translation stage and manually moved along the z (depth) axis.

3.2. z coordinate calibration

The translation stage was moved toward the structured light system and data was captured in 5 mm increments from $z_0=0$ mm (farthest point from camera and projector) to $z_{20}=100$ mm. 21 calibration planes were captured. Of the 21 planes, 11 and 6 evenly spaced planes in the z_0-z_{20} range were used for curve fitting with different curve fitting methods (i.e. linear interpolation and polynomial fitting). Due to lens distortion and other factors, the absolute phase-depth curve for each pixel varies, so a curve was fit to each similar pixel on the calibration planes. With the remaining planes, the average fitting error per plane was calculated for each curve fitting method by subtracting the captured depth value from the experimental value determined through the curve fitting.

The accuracy of z calibration was evaluated for four different curve fitting methods: linear interpolation, 2nd-, 3rd-, and 4th-order polynomials. The average depth calibration error was calculated when using evenly spaced calibration planes for curve fitting, but the amount of space between the calibration planes was changed. Fig. 3(a) shows calibration error for the four curve fitting methods when 11 interpolation planes were used. The planes were space 10 mm apart. Fig. 3(b) shows calibration error for the four curve fitting methods when 6 interpolation planes were used spaced 20 mm apart.

From the experimental results, linear interpolation, 3rd-, and 4th-order polynomials fit the absolute phase-depth relationship with reasonable accuracy; however, 3rd- and 4th order polynomials produce a slightly more accurate fitting method (a maximum absolute average depth error of 0.064 mm for 3rd-order polynomial compared with 0.098 mm obtained by linear interpolation).

As the number of calibration planes decreases, low-order polynomial curve fitting represents the z coordinate data significantly more accurately compared to linear interpolation. Fig. 3(b) shows the calibration depth errors when 6 interpolation planes were used. In this experiment, the maximum absolute average depth error for linear interpolation was 0.260 mm compared to 0.070 mm for 3rd-order polynomial. This is because the absolute phase-depth relationship is nonlinear, and if fewer calibration planes are used, the nonlinear effect is exaggerated and not well defined by linear interpolation.

For traditional sinusoidal fringe projection technique, it could be true that increasing the polynomial's order generates less error, albeit requires more calibration planes. However, for our

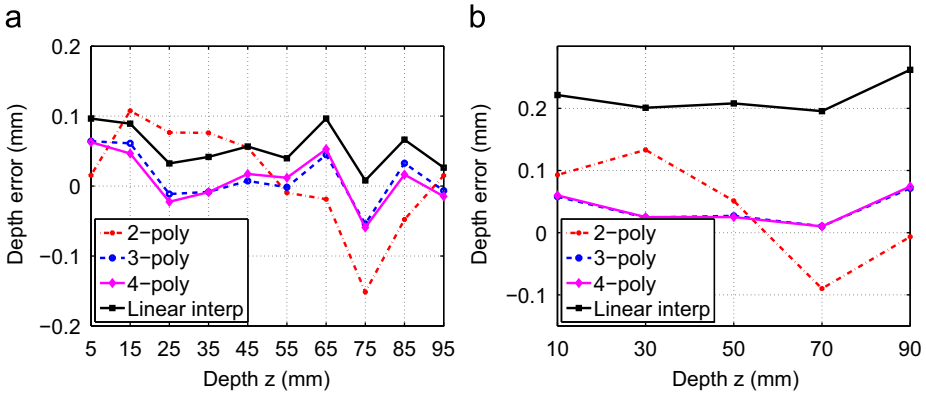

Fig. 3. Average depth error per plane using different curve fitting methods. (a) RMS error when 11 interpolation planes were used; (b) RMS error when 6 interpolation planes were used.

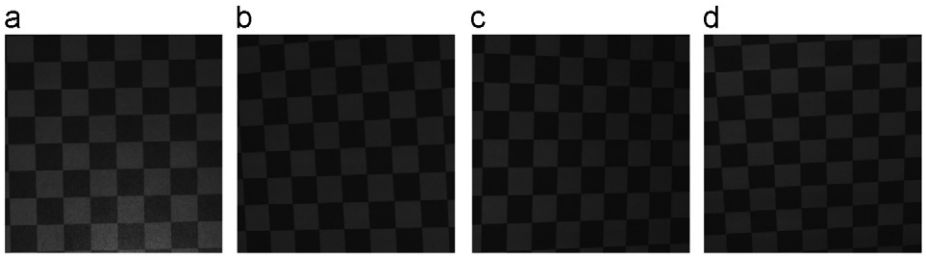

Fig. 4. Example of four images of plane used in camera calibration set at different angles.

binary defocusing technique, our experimental data showed that the error with 3rd-order polynomials already returns error close to that of the linear translation stage and using higher order polynomials will not lead to increased overall accuracy but will increase the depth z interpolation computation time and complexity. This finding was also experimentally verified by the prior study by Xu et al. [4]. Therefore, the remaining experiments curve fit using 3rd-order polynomials.

It should be noted that during the depth z calibration stage, the projected fringe patterns are monochromatic so that the red/blue checkers will not appear. The red/blue printed color contrast was previously calibrated based on the system setup to ensure that when the projector is projecting monochromatic images, the checkers disappear.

3.3. *x and y coordinate calibration*

After z calibration, x and y coordinates can be calibrated using the procedure explained in Section 2.4. The z_0 plane, located at 0 mm for z calibration, is manually adjusted in the algorithms to $z_0=50$ mm. This step is essential to unify the coordinate systems used in z calibration and x and y calibration. Then, the captured calibration plane at location z_0 used in z interpolation is set as the reference for Zhang's optimization procedure [15]. It is important to notice that during this stage of calibration, the red/blue checkerboard was illuminated with red light so that the checkers will appear as regular checkerboard. 11 more images of the red/blue checkerboard calibration plane are captured at different orientations for calibrating the intrinsic and extrinsic parameters (see Fig. 4). The intrinsic and extrinsic parameters were optimized using the 12 captured images in an optimization algorithm.

To test the calibration accuracy, four pixels in the corners on the checkerboard were chosen, as shown in Fig. 5. The top left corner pixel and the bottom right pixel forms Diagonal 1 (line AD). The other two corner pixels form Diagonal 2 (line BC). From

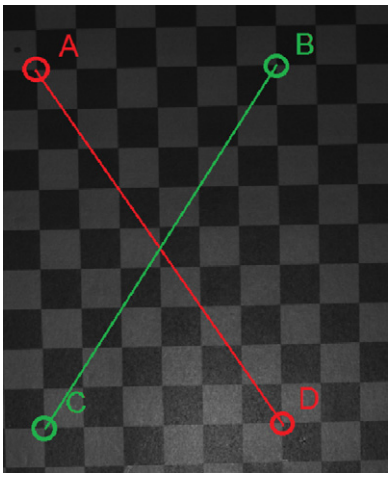

Fig. 5. The measured diagonals.

Eq. (7), (x, y, z) information of all the four corners can be obtained. Then the lengths of both diagonals can be calculated, as shown in Table 1.

From the results, the (x, y, z) coordinate measurement accuracy was fairly good: approximately 1.6% error. However, comparing with depth z accuracy, (x, y) calibration accuracy is much lower. Moreover, one might notice that the average values calculated from Eq. (7) are smaller than the measured values. This could be caused by the camera calibration error. The variation of Diagonal 2 is larger than Diagonal 1. This could result from the distortion of camera lens, which was not considered in our camera calibration algorithm. One should notice that the goal of this paper is to provide a more accurate calibration method for depth z; thus, z calibration was given higher priority. If one wants to increase (x, y) calibration as well, a better camera calibration approach could be adopted.

3.4. 3D shape reconstruction

To further verify the depth calibration accuracy, we also did an experiment to measure a step height object as shown in Fig. 6. Fig. 6(a) shows the photo of the object, and the 3D reconstruction result is shown in Fig. 6(b). The step height is about 40.00 mm measured by a digital caliper, while the calibrated result is 40.29 mm. The relative error is about 0.7%.

Table 1
Measurement accuracy verification for four corner points.

	Diagonal 1 (mm)	Diagonal 2 (mm)
1	134.51	134.52
2	134.16	135.93
3	134.08	136.43
4	134.80	133.36
5	135.33	132.86
6	136.33	132.55
7	135.94	137.90
8	135.39	137.28
9	135.26	136.59
10	134.05	132.22
11	134.00	133.06
12	134.33	135.93
Average	134.84	134.88
Variation	0.79	2.02
Measured[a]	137.01	137.18

[a] Values are obtained from a high-accuracy digital caliper.

Fig. 7 shows the 3D shape reconstruction of a sculpture. Fig. 7(a) shows one of the nine fringe patterns and Fig. 7(b) shows one of the coding patterns. Fig. 7(c) shows the extracted absolute phase map, and the recovered 3D result is shown in Fig. 7(d). Fig. 7 along with Fig. 6 demonstrate that the proposed calibration technique allows the 3D shape measurement system to accurately reconstruct 3D models with high resolution and accuracy.

4. Summary

We have presented a novel method for calibrating a structured light system using the binary defocusing technique. Our procedure curve fits z coordinate information between selected planes in a known range. x and y coordinates are then calibrated by an optimization procedure to find extrinsic and intrinsic camera parameters. With the proposed method, we have demonstrated that a 3D model be accurately reconstructed. Proper calibration of a structured light system using the defocusing technique may help to realize the advanced capabilities of defocusing technology over traditional sinusoidal fringe projection. This calibration method can also be adopted for traditional fringe projection techniques. It should be noted that badly defocused binary patterns will introduce significant phase errors that may couple and reduce measurement accuracy. For our experiments, we used binary patterns with a small pitch as well as nine-step phase shifting to reduce errors introduced by the high order harmonics

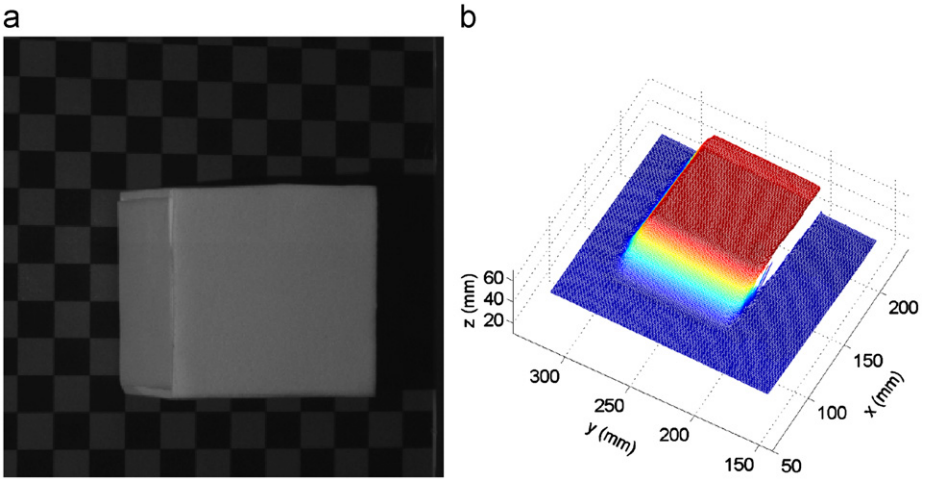

Fig. 6. 3D shape measurement result of a step-height object. (a) Step-height object; (b) 3D result.

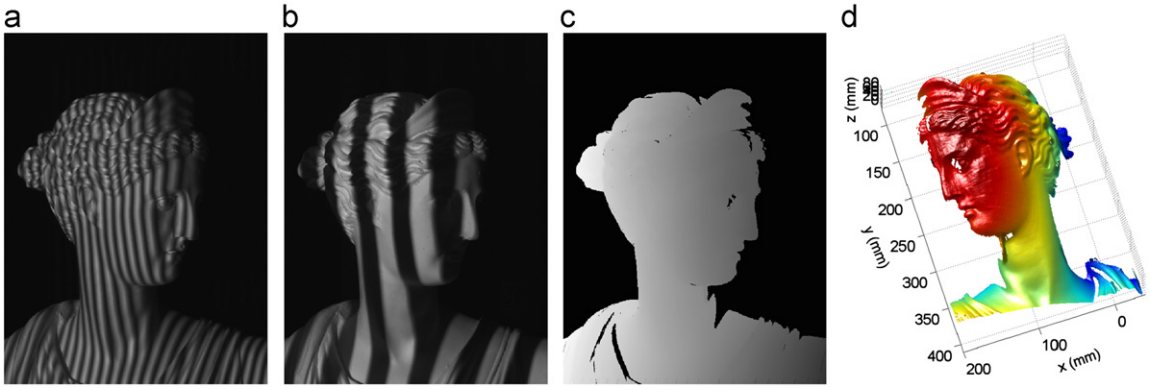

Fig. 7. 3D shape measurement results of complex object. (a) One fringe pattern; (b) One coding pattern; (c) Absolute phase map; (b) 3D reconstruction results.

present in binary patterns. Future work may combine phase error compensation with the proposed calibration technique.

Acknowledgment

This work was partially supported by the National Science Foundation under project number CMMI: 1150711.

References

[1] Zhang S. Recent progresses on real-time 3-D shape measurement using digital fringe projection techniques. Opt Laser Eng 2010;48(2):149–58.
[2] Lei S, Zhang S. Digital sinusoidal fringe generation: defocusing binary patterns VS focusing sinusoidal patterns. Opt Laser Eng 2010;48(5):561–9.
[3] Lei S, Zhang S. Flexible 3-D shape measurement using projector defocusing. Opt Lett 2009;34(20):3080–2.
[4] Xu Y, Ekstrand L, Dai J, Zhang S. Phase error compensation for three-dimensional shape measurement with projector defocusing. Appl Opt 2011;50(17):2572–81.
[5] Guo H, He H, Yu Y, Chen M. Least-squares calibration method for fringe projection prolometry. Opt Eng 2005;44:1–9.
[6] Huang L, Chua PSK, Asundi A. Least-squares calibration method for fringe projection profilometry considering camera lens distorsion. Appl Opt 2010;49:1539–48.
[7] Zhang S, Huang PS. Novel method for structured light system calibration. Opt Eng 2006;45(8):083,601.
[8] Yang R, Cheng S, Chen Y. Flexible and accurate implementation of a binocular structured light system. Opt Lasers Eng 2008;46(5):373–9.
[9] Gao W, Wang L, Hu Z. Flexible method for structured light system calibration. Opt Eng 2008;47(8):083,602.
[10] Li Z, Shi Y, Wang C, Wang Y. Accurate calibration method for a structured light system. Opt Eng 2008;47(5):053,604.
[11] Hu Q, Huang PS, Fu Q, Chiang FP. Calibration of a 3-D shape measurement system. Opt Eng 2003;42(2):487–93.
[12] Cuevas FJ, Servin M, Stavroudis ON, Rodriguez-Vera R. Multi-layer neural networks applied to phase and depth recovery from fringe patterns. Opt Commun 2000;181(4):239–59.
[13] Legarda-Sáenz R, Bothe T, Jüptner WP. Accurate procedure for the calibration of a structured light system. Opt Eng 2004;43(2):464–71.
[14] Zhang C, Huang PS, Chiang F-P. Microscopic phase-shifting profilometry based on digital micromirror device technology. Appl Opt 2002;41(8):5896–904.
[15] Zhang Z. A flexible new technique for camera calibration. IEEE Trans Pattern Anal Mach Intell 2000;22:1330–4.
[16] Bouguet J-Y. Camera Calibration ToolBox for Matlab, Online available at: 〈http://www.vision.caltech.edu/bouguetj/calib_doc〉.
[17] Malacara D, editor. Optical shop testing. 3rd ed.. New York: John Wiley and Sons; 2007.
[18] Ghiglia DC, Pritt MD. Two-dimensional phase unwrapping: theory, algorithms, and software. John Wiley and Sons Inc; 1998.
[19] Creath K. Step height measurement using two-wavelength phase-shifting interferometry. Appl Opt 1987;26:2810–6.
[20] Cheng Y-Y, Wyant JC. Multiple-wavelength phase shifting interferometry. Appl Opt 1985;24:804–7.
[21] Towers DP, Jones JDC, Towers CE. Optimum frequency selection in multi-frequency interferometry. Opt Lett 2003;28:1–3.
[22] Huntley JM, Saldner HO. Temporal phase-unwrapping algorithm for automated interferogram analysis. Appl Opt 1993;32:3047–52.
[23] Sansoni G, Carocci M, Rodella R. Three-dimensional vision based on a combination of gray-code and phase-shift light projection: analysis and compensation of the systematic errors. Appl Opt 1999;38(31):6565–73.
[24] Mao X, Chen W, Su X. Improved Fourier-transform profilometry. Appl Opt 2007;46:664–8.
[25] Zhang X, Lin Y, Zhao M, Niu X, Huang Y. Calibration of a fringe projection profilometry system using virtual phase calibrating model planes. J Opt A Pure Appl Opt 2005;7:192.
[26] Sitnik R, Ska MK, Nicki JW. Digital fringe projection system for large volume 360-deg shape measurement. Opt Eng 2002;41(2):443–9.